Thin Solid Films 731 (2021) 138748

Contents lists available at ScienceDirect

Thin Solid Films

journal homepage: www.elsevier.com/locate/tsf

Investigation into the electrodeposition of Ga-Fe-O thin films

A. Prados [a], A. Muñoz-Noval [a], R. Ranchal [a,b,*]

[a] Dpto. Física de Materiales, Facultad CC. Físicas. Universidad Complutense de Madrid. Plaza de las Ciencias 1, Madrid 28040, Spain
[b] Instituto de Magnetismo Aplicado, UCM-ADIF-CSIC, Las Rozas 28230, Spain

ARTICLE INFO

Keywords:
Electrodeposition
Magnetoelectricity
Gallium iron oxide

ABSTRACT

In this work we present an exhaustive investigation about the possibility of using the electrodeposition technique to grow Ga-Fe-O thin films. The morphological and structural characterization has been performed by means of scanning electron microscopy, X-ray diffractometry and X-ray absorption near edge structure measurements. These results have been complemented with chronoamperometric measurements recorded during growth. We have explored different electrolytes, growth potentials, and pH being observed that it is possible to tune the Fe/Ga ratio by means of the potential whereas the surface morphology is closely related to the Na_3-citrate content in the electrolyte. The surface roughness is reduced as the Fe content in the layer is increased upon the raise of citrate in the electrolyte composition. X-ray diffractometry indicates that Ga can become partially oxidized, whereas Fe seems to keep its metallic state in its vast majority since we have not obtained clear evidences of oxidation. Thus, this investigation highlights the inherent difficulties to synthetize Ga-Fe-O compounds by means of the electrodeposition technique.

1. Introduction

$GaFeO_3$ (GFO) oxides are of great interest mainly due to their magnetoelectric properties that were discovered in the last 60 s in bulk samples [1-2]. In the 2000s, GFO thin films started to be studied [3-7] due to the increasing interest on multiferroics. From the application point of view this material can represent a breakthrough due to its magnetoelectric properties that can be exploited in magnetic memories to reduce the energy consumption. In addition, GFO is a free-rare earth compound being therefore eco-friendly. Samples can be synthesized by different methods as floating-zone method [3], sol-gel [8-10], solid state route [11-15] or solid-state chemical reaction [16]. The inherent problems for the synthesis of this material system were highlighted when shown the necessity of a large optimization process in the solid state route [11].

GFO is a system with an orthorhombic $Pc2_1n$ structure (group number 33) for the composition range in which magnetoelectricity is observed [17]. High quality thin films have been obtained when using pulsed laser deposition [4,18-21]. In an effort to explore industrial processes to synthetize GFO, we have previously studied the structural and magnetic properties of Fe-Ga thin films during thermal treatments in oxygen atmosphere in a temperature range from 500 °C to 800 °C [22]. At 500 °C, we observed by X-ray absorption fine structure spectroscopy that the annealing promoted the formation of Ga-rich aggregates. At 600 °C, Ga becomes oxidized whereas Fe maintains its metallic state. Ga starts to evaporate at 700 °C leaving a Ga-poor layer that is eventually oxidized into α-Fe_2O_3. These results demonstrate the difficulties to use thermal oxidation to obtain GFO thin films.

Another interesting synthesis route with industrial applications is the electrodeposition. Reddy et al. reported the appearance of GFO oxides when trying to electrodeposit Fe-Ga alloys from citrate-based electrolytes for rotation rates ($\sqrt{\omega}$) lower than 15 $min^{1/2}$ on a rotating disc electrode [23]. In other work, the presence of oxygen was observed during the electrodeposition of metallic FeGa alloys for non-optimized growth conditions using a stirred electrolyte [24].

Taking into account that electrodeposition is one of the most widely used growth techniques in industrial applications, the motivation of this work is to explore possible routes for the electrodeposition of GFO. As a first approach, we have considered studies about FeGa electrodeposition in which oxides have been observed [23,24], since to our best knowledge no works about GFO electrodeposition have been published. For that reason, we have used stationary electrodes and non-stirred electrolytes. We have modified growth parameters as the electrolyte composition, growth potential, and pH around previously reported values that promote oxides during electrodeposition of FeGa thin films [23,24]. We have observed that to obtain flat thin films it is necessary to

* Corresponding author at: Dpto. Física de Materiales, Facultad de CC. Físicas. Plaza de las Ciencias 1, Madrid 28040, Spain.
E-mail addresses: rociran@ucm.es, rociran@fis.ucm.es (R. Ranchal).

https://doi.org/10.1016/j.tsf.2021.138748
Received 9 December 2020; Received in revised form 13 May 2021; Accepted 14 May 2021
Available online 23 May 2021

adjust the Na_3-citrate content. Modifying the growth potential enables to tune the Fe/Ga ratio, and the increase of pH favors the formation of Ga-oxides. Nevertheless, Fe keeps almost totally its metallic state for the wide range of growth conditions studied in this work.

2. Experimental techniques

Samples have been grown by electrodeposition using different water-based electrolytes in which the composition, pH and growth potential have been varied as indicated in Table 1. In all cases, $FeSO_4$ and $Ga_2(SO_4)_3$ were the source of Fe^{2+} and Ga^{3+} ions, respectively, Na_3-citrate is the antioxidant, and Na_2SO_4 has been used in some cases to increase the electrolyte conductivity [24]. Electrolytes were prepared with analytical grade chemicals and deionized water, and pH was adjusted by means of diluted NH_4OH (10% vol.). Substrates were Si (111) covered with evaporated Ti (20 nm) and Au (20 nm). A PalmSens EmStat3+Blue potentiostat was used to control the growths that were carried out in a three-electrode cell with a platinum mesh as counter electrode and a Ag/AgCl (3 M NaCl) reference electrode supplied by Bioanalytical Systems, Inc. (E_{eq} = 0.196 V vs. standard hydrogen electrode). In this study, all potentials are referred to this electrode. Electrochemical experiments were performed without agitation or magnetic stirring in non-rotating substrates at 300 K. The growth time was adjusted to reach a thickness of around 200 nm. To do that, we have used the Faraday's law:

$$Q = \frac{nF\rho}{M_{atom}} St \quad (1)$$

where Q is the electric charge measured in the cathode, n is the number of electrons involved in the reduction reaction, F is the Farady's constant (96,485,34 C/mol), ρ is the density of the electrodeposited material, S is the area of the sample, and t is the expected thickness. The sample thickness was measured after the growth with an Alphastep profiler. Measured layer thickness was in good agreement with the growth time adjusted by Faraday's law.

X-ray diffractometry (XRD) in the Bragg-Brentano configuration was performed in a Philips X'Pert MPD using the Cu K_α wavelength (1.54056 Å). For the analysis of the peaks we have used the files JCPDS: 00-006-0529, 00-056-1272, 00-006-0503, 00-041-1103 and 01-077-8316 to identify the Ga_2O_3 diffraction peaks, 00-001-1174 for Au, 00-006-0696 for FeGa, and 00-031-0540 for Ga. For FeGa we have considered that Ga is introduced in the bcc Fe matrix to formed metallic FeGa as we have previously observed [24], and for Ga we have complemented the information of the JCPDS file with the theoretical Ga diffraction pattern simulated with the Diamond program. We have used a JEOL JSM 6400 scanning electron microscope (SEM) to study the surface morphology. To do that, SEM work conditions were 20 kV and 80 mA. The same working conditions were used in the SEM microscope to measure the Fe and Ga content of the samples by means of Energy Dispersive X-ray Spectroscopy (EDS). X-ray absorption near edge structure (XANES) spectroscopy was carried out at BM25-Spline at the European Synchrotron (ESRF), and at BL22-CLAESS at ALBA synchrotron. The spectra were acquired at the Fe and Ga K-edges (around 7 and 10 keV, respectively). For each edge and sample, at least 3 scans in fluorescence yield mode were collected and merged to obtain spectra with reasonable quality. The data reduction was performed by employing the Demeter software [25,26].

3. Results and discussion

We have studied the influence of the Na_3-citrate content in the electrolyte keeping constant a pH of 4 (electrolyte I-a in Table 1) using a potential of −1.6 V to electrodeposit the samples. We have chosen this high cathodic potential since it favors the electrodeposition of Fe alloys with compositions close to the composition of the electrolyte [27,28]. The Na_3-citrate has a clear impact on the morphology of the samples as it can be observed in the SEM images (Fig. 1). For the lowest Na_3-citrate content (5 mM) there are observed unconnected elongated islands whose size increases for 15 mM of citrate. A further increase of the citrate in the electrolyte up to 35 mM enables the coalescence of the islands, and eventually, for a Na_3-citrate content of 50 mM it is achieved a compact thin film (Fig. 1). The rise of citrate in the electrolyte also influences on the composition of the samples as it increases the Fe content from almost null to around 18 at.% (Fig. 2a), which is the Fe content in the electrolyte (obtained as $[Fe^{2+}]/([Fe^{2+}]+[Ga^{3+}])$. This indicates that Fe^{2+} ions are rather sensitive to oxidation and /or precipitation, and the use of antioxidants as Na_3-citrate is mandatory for the incorporation of Fe into the layer.

The XRD patterns of these samples are presented in Fig. 3. It can be observed diffraction peaks related to metallic Ga and Fe-Ga, and also to Ga_2O_3 oxides. We have not found evidences of Fe oxides by XRD. The diffraction peaks related to Ga_2O_3 are slightly shifted to higher angles –between 0.1° and 0.2°– which can be taken as an indication of Fe inside the Ga_2O_3. In fact, the smaller Fe size in comparison to Ga can explain this introduction promoting the experimentally observed lattice distortion. The addition of citrate enhances the ⟨200⟩ texture for metallic Ga as indicated by the increase of the (200) and (400) peaks in detriment of the (021) (Fig. 3). In parallel, the peaks related to Ga_2O_3 are reduced as reflected by the decrease of the (006), and ($6\bar{0}1$) reflections. Thus, the increase of citrate seems to favor the electrodeposition of metallic Ga and to reduce the formation of Ga oxides. Around 44.4° we can observe a

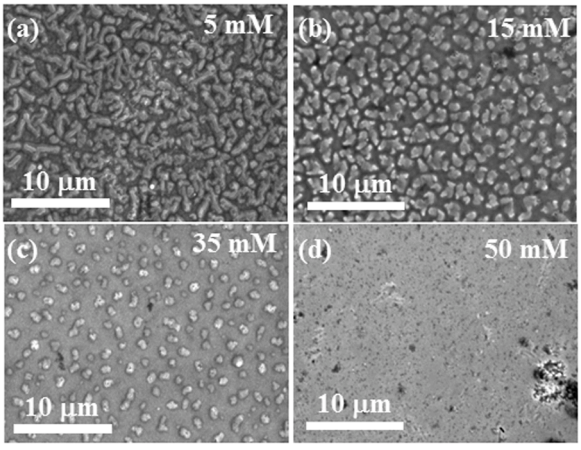

Fig. 1. Images obtained in a SEM microscope of the surface morphology for layers deposited with electrolyte I-a with different Na_3-citrate contents: (a) 5 mM, (b) 15 mM, (c) 35 mM, and (d) 50 mM.

Table 1
Summary of the electrolytes used in this work together with their composition, pH and applied overpotentials. Between brackets we present the range between the minimum and maximum value when a parameter has been modified.

Electrolyte	$FeSO_4$ (mM)	$Ga_2(SO_4)_3$ (mM)	Na_3-citrate (mM)	Na_2SO_4 (mM)	pH	Overpotential (V)
I-a	15	35	[5 – 50]	0.5	4	−1.6
I-b	15	35	[5 – 50]	0.5	6	- 1.6
II	15	35	50	—	4	[−1.2 – −1.6]
III	10	23	50	—	[4 – 8]	[−1.2 – −1.6]

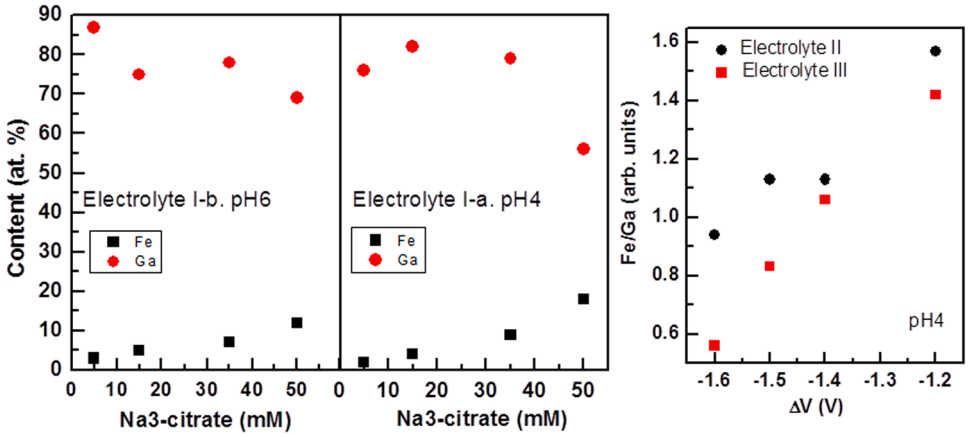

Fig. 2. Fe and Ga content in layers deposited with different Na_3-citrate contents: (a) electrolyte I-a, and (b) I-b. (c) Fe/Ga ratio for layers deposited at different overpotentials for electrolytes II (●) and III (■) with a pH = 4.

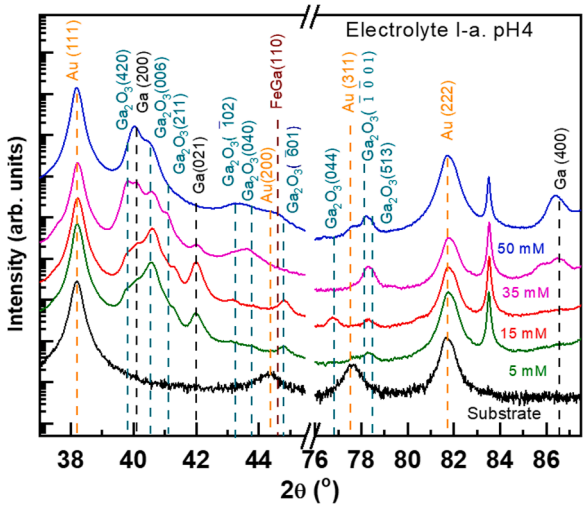

Fig. 3. X-ray diffraction patterns of samples deposited with electrolyte I-a with different Na_3-citrate contents for a pH = 4. Curves are vertically shifted for clarity.

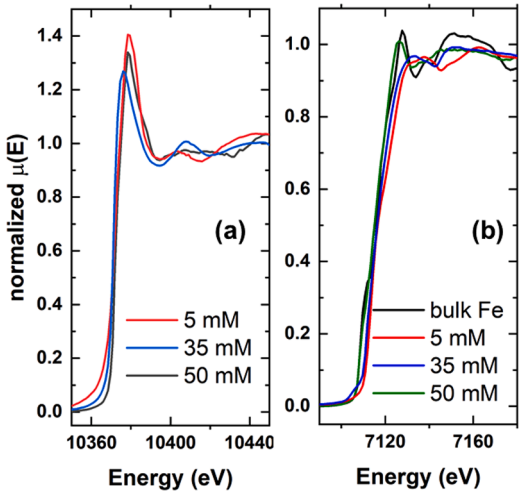

Fig. 4. (a) Ga-K edge and (b) Fe-K edge corresponding to experimental XANES spectra for samples deposited from electrolyte I-a with different Na_3-citrate contents.

somehow rather broad peak related to either the Au layer from the substrate, Ga_2O_3, and metallic FeGa. The increase of this peak with the addition of citrate that promotes the increase of Fe content inside the layer (Fig. 2a) indicates that this peak is related to FeGa alloys. Experimental XRD patterns only show one diffraction peak for metallic FeGa, reflection (110), whereas Ga_2O_3 is segregated with many different orientations. This can explain the reduction of the surface roughness when Fe is more favorable incorporated in the layers.

To get a deeper insight into the oxidation state of Ga and Fe, we have performed XANES spectroscopy since it provides information about the chemical state at the local range (Fig. 4a and for the metallic Ga reference see [22]). Regardless of the citrate content, it is observed that the experimental XANES spectra obtained at the Ga K-edge are distorted with respect to Ga metallic due to the formation of Ga oxides. When the citrate content is increased from 5 to 35 mM, the main peak (also defined as white line) shifts to lower energies, which might be a sign of decreasing the oxidation state. Therefore, the increase of citrate concentration in the electrolyte seems to inhibit the formation of Ga oxide and favors the reduction of metallic Ga, in agreement with the XRD results (Fig. 3). In Fig. 4b we present the experimental XANES spectra obtained at the Fe K-edge. They do not exhibit indications of oxidation apart from some distortions with respect to the metallic Fe spectra (for Fe reference see [29]) that can be related to structural disorder. Thus, Fe remains in its vast majority in metallic state.

All these experimental results showing the effect of the citrate content can be understood considering the codeposition process for FeGa alloys in citrate-based electrolytes proposed by Reddy et al. [23,30]. In fact, we can use these two references [23] and [30] to understand the growth process. In the first step of the codeposition process (the rate-determining step) Fe(II) ions are partially reduced into an adsorbed intermediate $[Fe(I)]_{ads}$ that involves the formation of a complex with the citrate (reaction 2).

$$Fe(II)^{-2} + HCit^{-} + e^{-} \rightarrow [Fe(I)HCit]^{-2}_{ads} \quad (2)$$

In the second fast step of the FeGa codeposition process, the unstable $[Fe(I)]_{ads}$ adsorbed complex can follow two possible routes: a) be reduced to metallic Fe(s) (reaction 3), or b) to induce the reduction of Ga (III) by first forming a mixed $[Ga(III)–Fe(I)]_{ads}$ adsorbed intermediate (reaction 4a), followed by its reduction to metallic Ga(s) (reaction 4b) or metallic FeGa(s) (reaction 4c) [23]. Then, the formation of FeGa oxides can happen by the reaction of FeGa(s) with water molecules.

$$[Fe(I)HCit]^{-2}_{ads} + e^{-} \rightarrow Fe(s) + HCit^{-3} \quad (3)$$

$$Ga(III) + [Fe(I)HCit]^{-2}_{ads} \rightarrow [Fe(I)Ga(III)HCit]^{+}_{ads} \quad (4a)$$

$$[Fe(I)Ga(III)HCit]^{+}_{ads} + ne^{-} \rightarrow Ga_{(s)} + [Fe(I)HCit]^{-2}_{ads} \quad (4b)$$

$$[Fe(I)Ga(III)HCit]^{+}_{ads} + ne^{-} \rightarrow FeGa_{(s)} + HCit^{-} \quad (4c)$$

However, Ga(III) ions can also follow parallel routes to form metallic Ga (reaction 5), or Ga hydroxides (reaction 6) that can also be transformed in oxides.

$$Ga(III) + 3e^{-} \rightarrow Ga \quad (5)$$

$$Ga(III) + 3OH^{-} \rightarrow Ga(OH)_3 \quad (6)$$

Therefore, when the concentration of Na_3-citrate is low in the electrolyte, $[Fe(I)]_{ads}$ is not produced and Fe cannot be introduced in the deposit (reaction 2). In addition, Ga(III) cannot follow reaction 4 (a-c) and is reduced into metallic Ga (reaction 5) and Ga hydroxides (reaction 6). Moreover, in the absence of a complexing agent for Ga^{3+} and a pH higher than 3.2, Ga^{3+} forms $GaOH^{2+}$ or GaO^{+} favoring the formation of Ga oxides in the film [30]. The higher the Na_3-citrate concentration in the electrolyte, the higher the $[Fe(I)]_{ads}$ with the following consequences: i) there is a higher incorporation of Fe in the deposited layer (Fig. 2a), ii) there is a detriment of Ga in the layer because $[Fe(I)]_{ads}$ competes with gallium ions for available surface sites on the electrode (Fig. 2a), and iii) Ga(III) are reduced into metallic Ga(s) or metallic FeGa by the catalytic effect of $[Fe(I)]_{ads}$, reducing the formation of Ga oxides and hydroxides (Fig. 3).

We have also studied a series of layers deposited with different Na_3-citrate contents but for a pH of 6 (electrolyte I-b) in order to favor the formation of oxides by increasing the content of OH^{-} ions. We have observed the same influence of the citrate in the morphology of these samples and similar diffraction patterns. Thus, pH seems not to have a clear impact for these growth conditions. For electrolyte I-b (Fig. 2b), the incorporation of Fe in the layers is also rather low except when the Na_3-citrate concentration is increased as also obtained in electrolyte I-a. Therefore, increasing the pH from 4 to 6 does not significantly influence either in the codeposition process described in Eqs. (2)-4 or in the formation of Ga hydroxides (reaction 6).

Taking into account the previous results, we decided to focus our efforts on high concentrated Na_3-citrate (50 mM) electrolytes to synthesize compact layers. In addition, from hereafter we will only present results for electrolytes without Na_2SO_4 (electrolytes II and III in Table 1) since the absence of a pH buffer produces a local depletion of H^{+} at the cathode surface that causes a local increase in pH that favors the formation of Fe-Ga oxides [30]. With electrolyte II we have studied the influence of the growth potential around values previously reported ranging from −1.2 to −1.6 V [23-24]. In the chronoamperometric measurements recorded during the growth (Fig. 5) it can be observed an increase of the current density as the overpotential is more negative being possible to achieve the 200 nm nominal thickness in less time. In general, a steady value for the current density is obtained after the nucleation process except for the highest studied overpotential. In Fig. 6 it can be observed that the surface roughness is pretty low regardless of the potential as expected from the use of 50 mM Na_3-citrate in the electrolyte. Moreover, the incorporation of Fe inside the layers is higher than with the electrolytes I (a and b) as indicated by the higher Fe/Ga ratio (Fig. 2). This suggests an inhibiting effect of Na_2SO_4 in the formation of the intermediate $[Fe(I)]_{ads}$. For all the studied potentials, the Fe/Ga ratio in the layers is always higher than the ratio in the electrolyte ($[Fe^{2+}]/[Ga^{3+}] = 0.43$). It is also possible to control the Fe/Ga ratio by means of the growth potential around the desired value of 1 in order to eventually reach the $Ga_{0.2}Fe_{0.2}O_{0.6}$ compound (Fig. 2c).

Nevertheless, the diffraction patterns of these samples (Fig. 7a) clearly show the absence of any kind of oxide, and we can only correlate the diffraction peaks to metallic Fe-Ga alloys. The sample deposited at −1.6 V seems to have a less intense diffraction peak for the FeGa(110) reflection. We correlate this effect to the different chronoamperometric measurement obtained for this sample.

To confirm the metallic state of both Fe and Ga, we have performed XANES at their K-edges (Figs. 8a and b). The experimental spectra in both edges only exhibit some small distortions with respect to the metallic cases pointing out the absence of oxides in these layers. As the Fe/Ga ratio was around the correct value, we have tried to oxidize these layers by immersing them inside 0.5 M KOH for 3 h at room temperature. However, the XRD patterns (Fig. 7b) are not modified by this chemical treatment reflecting the high chemical stability of these samples at least at 300 K.

Since with electrolyte II the layers are flat and the relative content between Fe and Ga is close to one, we have investigated the use of another electrolyte (electrolyte III) in which the content of $FeSO_4$ and $Ga_2(SO_4)_3$ is modified (Table 1) in order to avoid the routes to produce metallic FeGa (reaction 4c) and Ga (reaction 4b). Similarly to electrolyte II, with electrolyte III it is possible to obtain flat films as shown in Fig. 9a, and b. The chronoamperometric measurements presented in Fig. 9c indicate that for this electrolyte there is a lower influence of the overpotential on the current density in comparison to electrolyte II. With electrolyte II current density is modified from around −4 mA·cm^2 for −1.2 V to ca. −29 mA·cm^2 for −1.6 V (Fig. 5), whereas with electrolyte III at pH4 it ranges from close to −2.5 mA·cm^2 for −1.2 V to around −13 mA·cm^2 for −1.6 V (Fig. 9c). For this electrolyte III and overpotentials of −1.2 V and −1.4 V it is reached a steady value for the current density, whereas for −1.5 V and −1.6 V, there is an increase of the current density once the nucleation has taken place. This behavior is similar but more pronounced than what it was observed in electrolyte II at −1.6 V.

The XRD patterns related to these samples deposited with electrolyte

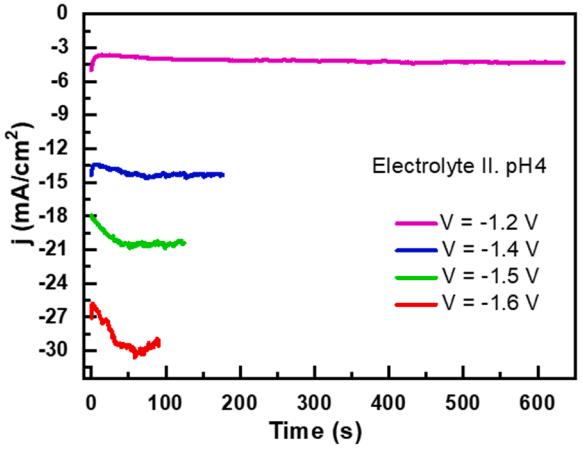

Fig. 5. Chronoamperometric measurements y for samples deposited from electrolyte II at different overpotentials.

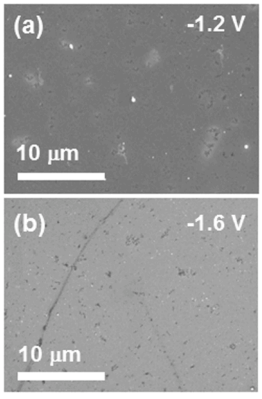

Fig. 6. Images obtained in a SEM microscope of the surface morphology for samples deposited from electrolyte II at different overpotentials (a) −1.2 V and (b) −1.6 V.

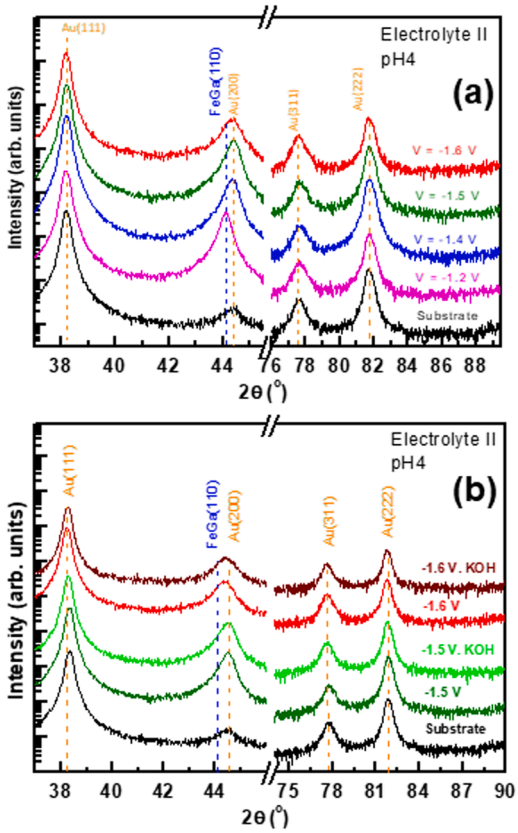

Fig. 7. (a) X-ray diffraction patterns of samples deposited from electrolyte II at different overpotentials. (b) Comparison of x-ray diffraction patterns of samples deposited from electrolyte II at different overpotentials and after being immersed in 0.5 M KOH during 3 h. Curves are vertically shifted for clarity.

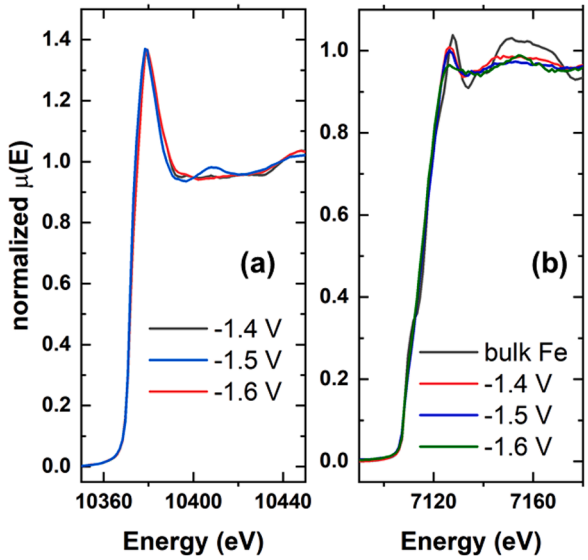

Fig. 8. (a) Ga-K edge and (g) Fe-K edge corresponding to XANES spectra for samples presented in Fig. 7(a).

III (Fig. 10) reveal that they are formed by metallic Ga and Fe-Ga phases, with Fe/Ga ratios also around 1 as it is shown in Fig. 2c. However, when using high overpotentials, −1.5 and −1.6 V, to electrodeposit the layers, Ga oxides are also detected by means of XRD, indicating an inhibition of the routes to produce metallic FeGa (reaction 4c) and Ga (reaction 4b). This could be a result of the stabilization of Ga hydroxide phases

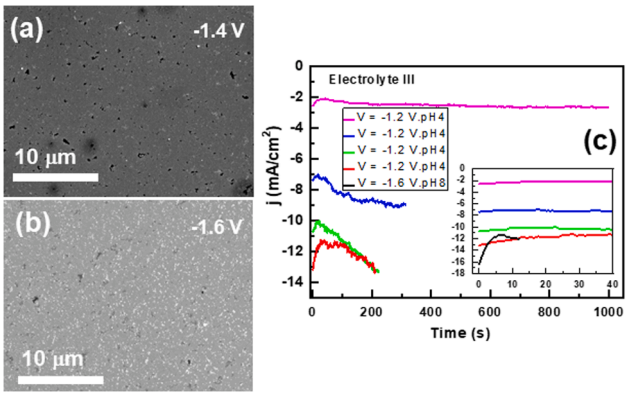

Fig. 9. SEM images of samples deposited from electrolyte III with a pH = 4 at different overpotentials, (a) −1.4 V, and (b) −1.6 V, respectively. (c) Chronoamperometric measurements recorded during the growth of samples deposited from electrolyte III with pH = 4 at different overpotentials. In the inset it is included the chronoamperometric measurement for a pH = 8.

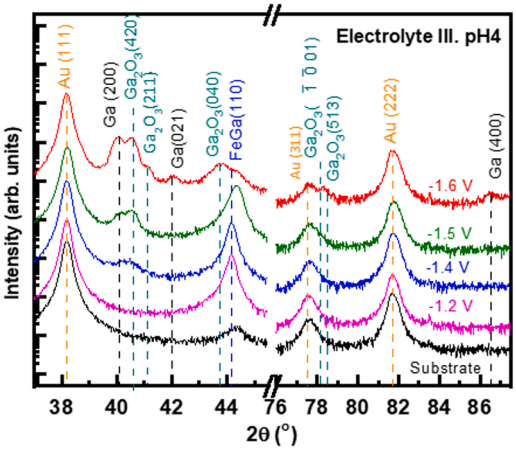

Fig. 10. X-ray diffraction patterns of samples deposited from electrolyte III with a pH = 4 at different overpotentials. Curves are shifted for clarity.

produced by the pH rise caused near the substrate surface by water reduction [30]. In fact, the chronoamperometric measurements were different not showing a steady value for the current density for these two overpotentials, −1.5 V and −1.6 V. The increase of the potential to more negative values reduces the diffraction peak related to metallic Fe-Ga (Fig. 10) decreasing the Fe incorporated in the layer (Fig. 2c). Electrodepositing with more negative potentials also enhances the diffraction peaks related to Ga in either metallic or oxidized state (Fig. 10). This can be partially understood considering the higher incorporation of Ga detected by EDS as the potential becomes more negative (Fig. 2c). If we combine the XRD results for this electrolyte (Fig. 10) with the corresponding chronoamperometric measurements (Fig. 9c), it seems that the absence of a steady current it is related to the inhibition of the route to produce metallic FeGa. In fact, a similar result has been obtained with electrolyte II. For this electrolyte and using −1.6 V, the chronoamperometry reveals the absence of a steady current being in this case reduced the formation of metallic FeGa (Fig. 7a). In order to confirm the oxidation state of Ga and Fe, we have performed XANES at their K-edges in these samples (Fig. 11). Again, XANES spectra mainly show features related to metallic Fe and Ga ruling out a clear oxidation state in none of them, remaining in a large proportion in the metallic state.

Since we have managed to grow flat films with a Fe/Ga ratio around 1 with electrolyte III, we have explored the possibility of enhancing the oxidation state of Fe by increasing the pH from 4 up to 8. In this case, the

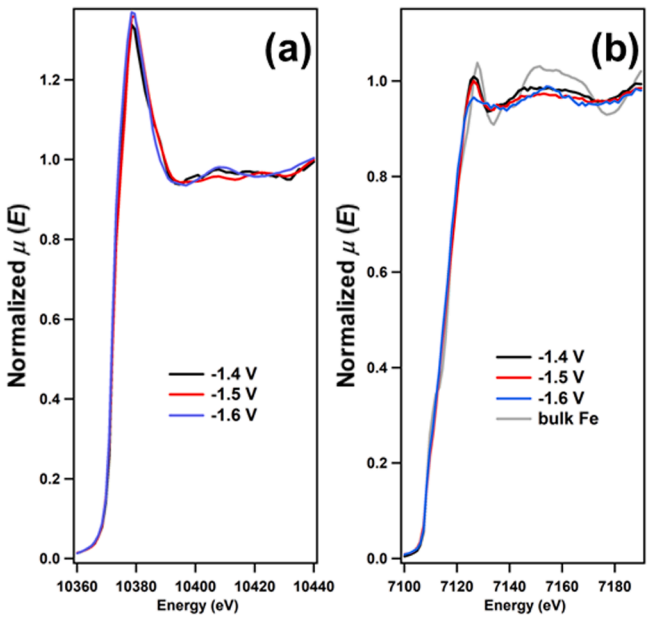

Fig. 11. (a) Ga-K edge and (b) Fe-K edge corresponding to XANES spectra for samples deposited at different overpotentials from electrolyte III.

chronoamperometric evidence a higher growth rate especially when using a pH of 8 (Inset, Fig. 9 c). This high growth rate makes not possible to observe the increase of the current density present for samples deposited with a pH of 4 once the nucleation has taken place. The XRD of the samples deposited at different pH are presented in Fig. 12a. Again, they show a clear presence of metallic Ga in all cases. The increase of pH to 8 seems to decrease the metallic Ga being favored Ga_2O_3 oxides due to the promotion of reaction 6 by the increase of [OH^-]. The surface morphology is flat (Fig. 12b and c) being not observed a significant effect of pH. In any case, there is still a rather large contribution of metallic FeGa on the diffraction pattern of that sample, and no GFO is detected. Thus, increasing the pH seems not to be an option to obtain GFO, at least for these growth conditions.

Therefore, the growth conditions investigated in this work are not appropriate to synthesize GFO compounds since in the most positive scenario, when Ga is oxidized, we have observed large indications of phase segregation with metallic FeGa alloys. These results are in agreement with reports about thermal oxidation that show that it was not possible to completely oxidized FeGa thin films because Ga prevents Fe oxidation [22]. In the experiments performed in this work we have observed that neither the increase of the electrolyte's pH or even the use of KOH baths can promote the oxidation of Fe in order to synthesize GFO compounds. It has been reported that Ga solution in Fe can prevent the macro-oxidation [31] being necessary to avoid the formation of metallic FeGa to enhance the formation of GFO. The possibility of electrodepositing GFO still remains an open question.

4. Conclusions

We have explored the possibility of using the electrodeposition technique to synthesize GFO thin films. First of all, we have observed that the citrate content in the electrolyte has a clear impact on the surface morphology being possible to grow flat layers for 50 mM of citrate in the electrolyte. On the other hand, the Fe/Ga ratio can be tuned around 1 by means of the growth potential. Ga_2O_3 oxides have been observed by means of XRD for some growth conditions, but there is also a great amount of Ga in its metallic state as pointed out by XANES. Fe is mainly detected in its metallic state by XANES with indications of FeGa alloys obtained by XRD. Therefore, the experimental results reflect the inherent difficulties of electrodepositing GFO.

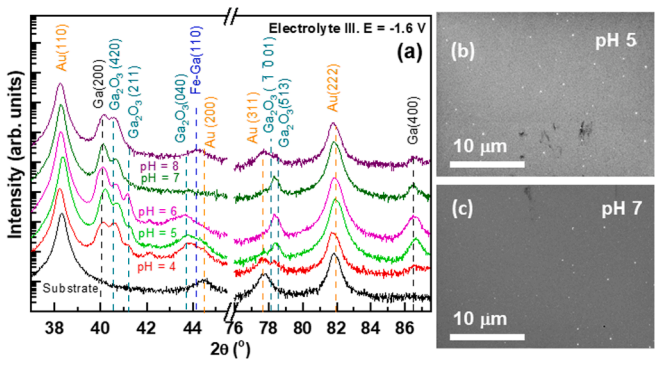

Fig. 12. (a) X-ray diffraction patterns of samples deposited from electrolyte III with an overpotential of −1.6 V but different pHs. Curves are vertically shifted for clarity. Images of the surface morphology obtained in a SEM microscope for (b) pH = 5, and (c) pH = 7.

CRediT authorship contribution statement

A. Prados: Conceptualization, Investigation, Formal analysis, Writing - review & editing. **A. Muñoz-Noval:** Investigation, Formal analysis, Writing - review & editing. **R. Ranchal:** Conceptualization, Formal analysis, Funding acquisition, Writing - original draft, Writing - review & editing, Supervision.

Declaration of Competing Interest

The authors declare that they have no known competing financial interests or personal relationships that could have appeared to influence the work reported in this paper.

Acknowledgements

We thank 'CAI Difracción de rayos-X' of UCM for X-ray diffractometry measurements, and ICTS Centro Nacional de Microscopía of UCM for SEM characterization. We also acknowledge beamtime at BM-25A at the European Synchrotron (ESRF), and at BL22-CLAESS at ALBA synchrotron. This work has been financially supported through the projects MAT2015-66888-C3-3-R (MINECO/FEDER) and RTI2018-097895-B-C43 of the Spanish Ministry of Economy and Competitiveness. A. P. would like to acknowledge the postdoctoral fellowship granted by *Consejería de Educación, Juventud y Deporte* of *Comunidad de Madrid* and the European Social Fund (grant PEJD-2016/IND-2233 of the YEI program).

References

[1] G.T. Tado, Observation and possible mechanisms of magnetoelectric effects in a ferromagnet, Phys. Rev. Lett. 13 (1964) 335–337.
[2] S.C. Abrahams, J.M. Reddy, J.L. Bernstein, Crystal Structure of Piezoelectric Ferromagnetic Gallium Iron Oxide, J. Chem. Phys. 42 (1965) 3957–3968.
[3] T. Arima, D. Higashiyama, Y. Kaneko, J.P. He, T. Goto, S. Miyasaka, T. Kimura, K. Oikawa, T. Kamiyama, R. Kumai, Y. Tokura, Structural and magnetoelectric properties of $Ga_{2-x}Fe_xO_3$ single crystals grown by a floating-zone method, Phys. Rev. B 70 (2004), 064426.
[4] M. Trassin, N. Viart, G. Versini, S. Barre, G. Pourroy, J. Lee, W. Jo, K. Dumesnil, C. Dufour, S. Robert, Room temperature ferrimagnetic thin films of the magnetoelectric $Ga_{2-x}Fe_xO_3$, J. Mater. Chem. 19 (2009) 8876–8880.
[5] S. Mukherjee, A. Roy, S. Auluck, R. Prasad, R. Gupta, A. Garg, Room temperature nanoscale ferroelectricity in magnetoelectric $GaFeO_3$ epitaxial thin films, Phys. Rev. Lett. 111 (2013), 087601.
[6] S.H. Oh, J.H. Lee, R.H. Shin, Y. Shin, C. Meny, W. Jo, Room-temperature polarization switching and antiferromagnetic coupling in epitaxial $(Ga,Fe)_2O_3$/$SrRuO_3$ heterostructures, Appl. Phys. Lett. 106 (2015), 142902.
[7] M. Bakr Mohameda, A. Senyshyna, H. Ehrenberga, H. Fuess, Structural, magnetic, dielectric properties of multiferroic $GaFeO_3$ prepared by solid state reaction and sol–gel methods, J. Alloys Compnd. 492 (2010) L20–L27.
[8] M. Mishra, A. Roy, A. Garg, R. Gupta, S. Mukherjee, Room temperature multiferroism in polycrystalline thin films of gallium ferrite, J. Alloys Compn. 721 (2017) 593–599.

[9] J. Sánchez., D.A. Cortés-Hernández, J.C. Escobedo-Bocardo, R.A. Jasso-Terán, A. Zugasti-Cruz, A. magnetic nanoparticles of Fe–Ga synthesized by sol–gel for their potential use in hyperthermia treatment, J. Mater. Sci.: Mater. Med. 25 (2014) 2237–2242.
[10] X. Sun, D. Tiwari, D.J. Fermin, High interfacial hole-transfer efficiency at $GaFeO_3$ thin film photoanodes, Ad. Energy Mater. 2002784 (2020), https://doi.org/10.1002/aenm.202002784.
[11] F. Roulland, C. Lefevre, A. Thomasson, N. Viart, Study of $Ga_{(2-x)}Fe_xO_3$ solid solution: optimisation of the ceramic processing, J. Eur. Ceram. Soc. 33 (2013) 1029–1035.
[12] B. Kundys, F. Roulland, C. Lefèvre, C. Mény, A. Thomasson, N. Viart, Room temperature polarization in the ferrimagnetic $Ga_{2-x}Fe_xO_3$ ceramics, J. Eur. Ceram. Soc. 35 (2015) 2277–2281.
[13] N. Wang, F. S.Wen, L. Li, Y. F.Lü, S. C.Liu, Y.F. Lu, Z. Y.Liu, J.L.He B.Xu, D. L.Yu, Y. J.Tian, Magnetic frustration effect in polycrystalline $Ga_{2-x}Fe_xO_3$, J. Magn. Magn. Mater. 322 (2010) 3595–3600.
[14] W. Kim, J.H. We, S.J. Kim, C.-.S. Kim, Effects of cation distribution for $AFeO_3$ (A = Ga, Al), J. Appl. Phys. 101 (2007) 09M515.
[15] S. Roy, B. Mallesham, V.B. Zade, A. Martinez, V. Shutthanandan, S. Thevuthasan, C.V. Ramana, Correlation between structure, chemistry, and dielectric properties of iron-doped gallium oxide ($Ga_{2-x}Fe_xO_3$), J. Phys. Chem. C 122 (2018) 27597–27607.
[16] S. Roy, C.V. Ramana, Effect of thermochemical synthetic conditions on the structure and dielectric properties of $Ga_{1.9}Fe_{0.1}O_3$ compounds, Inorg Chem 57 (2018) 1029–1039.
[17] S.C. Abrahams, J.M. Reddyand, J.L. Bernstein, Crystal structure of piezoelectric ferromagnetic gallium iron oxide, J. Chem. Phys. 42 (1965) 3957–3968.
[18] M. Trassin, N. Viart, G. Versini, J.-.L. Loison, J.-.P. Vola, G. Schmerber, O. Crégut, S. Barre, G. Pourroy, J.H. Lee, W. Jo, C. Mény, Epitaxial thin films of multiferroic $GaFeO_3$ on conducting indium tin oxide (001) buffered yttrium-stabilized zirconia (001) by pulsed laser deposition, Appl. Phys. Lett. 91 (2007), 202504.
[19] K. Sharma, V. Raghavendra Reddy, A. Gupta, R.J. Choudhary, D.M. Phase, V. Ganesan, Study of site-disorder in epitaxial magneto-electric $GaFeO_3$ thin films, Appl. Phys. Lett. 102 (2013), 212401.
[20] Zhong, Y. Bitla, J. Wang, X. Zhong, F. An, Y.-.Y. Chin, Y. Zhang, W. Gao, Y. Zhang, A. Eshghinejad, E.N. Esfahani, Q. Zhu, C. Tan, X. Meng, H.-.J. Lin, X. Pan, S. Xie, Y.-.H. Chu, J. Li, Tuning Fe concentration in epitaxial gallium ferrite thin films for room temperature multiferroic properties, Acta Mater 145 (2018) 488–495.
[21] T. Katayama, S. Yasui, Y. Hamasaki, M. Itoh, Control of crystal-domain orientation in multiferroic Ga0.6Fe1.4O3 epitaxial thin films, Appl. Phys. Lett. 110 (2017), 212905.
[22] P. Alvarez-Alvarez, A. Prados, A. Muñoz-Noval, R. Ranchal, Morphological, structural and magnetic evolution of sputtered $Fe_{70}Ga_{30}$ thin films upon annealing in oxygen atmosphere, J. Alloys Compnd. 713 (2017) 229–235.
[23] K.S.M. Reddy, E.C. Estrine, D.-.H. Lim, W.H. Smyrl, B.J.H. Stadler, Controlled electrochemical deposition of magnetostrictive $Fe_{1-x}Ga_x$ alloys, Electrochem commun 18 (2012) 127–130.
[24] R. Ranchal, D. Maestre, Growth and characterization of $Fe_{1-x}Ga_x$ thin films from citrate-based electrolytes, J. Phys. D 47 (2014), 355004.
[25] B. Ravel, M. Newville, ATHENA, ARTEMIS, HEPHAESTUS: data analysis for X-ray absorption spectroscopy using IFEFFIT, J. Synchrotron Rad. 12 (2005) 537–541.
[26] A.L. Ankudinov, B. Ravel, J.J. Rehr, S.D. Conradson, Real-space multiple-scattering calculation and interpretation of X-ray-absorption near-edge structure, Phys. Rev. B 58 (1998) 7565.
[27] A. Llavona, L. Pérez, M.C. Sánchez, V. de Manuel, Enhancement of anomalous codeposition in the synthesis of Fe–Ni alloys in nanopores, Electrochim. Acta 106 (2013) 392–397.
[28] X. Liu, G. Zangari, M. Shamsuzzoha, Structural and magnetic characterization of electrodeposited, high moment feconi films, J. Electrochem. Soc. 150 (2003) C159–C168.
[29] A. Muñoz-Noval, A. Ordóñez-Fontes, R. Ranchal, Influence of the sputtering flow regime on the structural properties and magnetic behavior of Fe-Ga thin films (Ga ~ 30 at.%), Phys. Rev. B 93 (2016), 214408.
[30] B.J.H. Stadler, K.S.M. Reddy, D.A. Rekenthaler, Electro-Chemical-Deposition of Galfenol and the Uses there Of, US Patent: 2012/0143046 A1 (2012).
[31] Q. Xing, M.J. Kramer, D. Wu, T.A. Lograsso, Influence of surface oxidation on transmission electron microscopy characterization of Fe–Ga alloys, Mater. Charact. 61 (2010) 598.